

Herschel/PACS far-infrared photometry of two $z > 4$ quasars^{*}

C. Leipski¹, K. Meisenheimer¹, U. Klaas¹, F. Walter¹, M. Nielbock¹, O. Krause¹, H. Dannerbauer², F. Bertoldi³, M.-A. Besel¹, G. de Rosa¹, X. Fan⁴, M. Haas⁵, D. Hutsemekers⁶, C. Jean⁷, D. Lemke¹, H.-W. Rix¹, and M. Stickel¹

¹ Max-Planck Institut für Astronomie (MPIA), Königstuhl 17, D-69117 Heidelberg, Germany e-mail: leipski@mpia-hd.mpg.de

² Service d'Astrophysique (SAP)/IRFU/DSM/CEA Saclay - Bât. 709, 91191 Gif-sur-Yvette Cedex, France

³ Argelander Institut für Astronomie, Universität Bonn, Auf dem Hügel 71, 53121 Bonn, Germany

⁴ Steward Observatory, University of Arizona, Tucson, AZ 85721, USA

⁵ Astronomisches Institut Ruhr-Universität Bochum, Universitätsstraße 150, 44801 Bochum, Germany

⁶ Institut d'Astrophysique et de Géophysique, University of Liège, Allé du 6 Août 17, 4000 Liège, Belgium

⁷ Instituut voor Sterrenkunde, Katholieke Universiteit Leuven, Celestijnenlaan 200B, 3001 Heverlee, Belgium

ABSTRACT

We present *Herschel* far-infrared (FIR) observations of two sub-mm bright quasars at high redshift: SDSS J1148+5251 ($z = 6.42$) and BR 1202–0725 ($z = 4.69$) obtained with the PACS instrument. Both objects are detected in the PACS photometric bands. The *Herschel* measurements provide additional data points that constrain the FIR spectral energy distributions (SEDs) of both sources, and they emphasise a broad range of dust temperatures in these objects. For $\lambda_{\text{rest}} \lesssim 20 \mu\text{m}$, the two SEDs are very similar to the average SEDs of quasars at low redshift. In the FIR, however, both quasars show excess emission compared to low- z QSO templates, most likely from cold dust powered by vigorous star formation in the QSO host galaxies. For SDSS J1148+5251 we detect another object at $160 \mu\text{m}$ with a distance of $\sim 10''$ from the QSO. Although no physical connection between the quasar and this object can be shown with the available data, it could potentially confuse low-resolution measurements, thus resulting in an overestimate of the FIR luminosity of the $z = 6.42$ quasar.

Key words. Galaxies: active; Galaxies: high-redshift; Infrared: galaxies

1. Introduction

The detection of large quantities of cold dust in high redshift ($z > 5$) quasars (e.g. Bertoldi et al. 2003; Beelen et al. 2006; Wang et al. 2008) implies a substantial enrichment of the interstellar medium already during the first billion years after the Big Bang. If the far-infrared (FIR) emission of these objects is powered by star-formation, then the luminosity and the temperature of the dust implies star formation rates of up to a few thousand solar masses per year, possibly indicating the rapid formation of early galactic bulges. Recent observations at mid-infrared (MIR) wavelengths with *Spitzer* demonstrated that the dust also shows an energetically important hot ($T \sim 1000$ K) component in many high-redshift QSOs (Hines et al. 2006; Jiang et al. 2006), with only few exceptions (Jiang et al. 2010). The similarity of the spectral energy distributions (SEDs) to those of lower redshift AGN lead to the conclusion that the general structures characterising local AGN are already in place at $z \sim 6$. However, for a majority of the sources the (sub)mm and MIR observations have only measured the tail of the dust emission spectrum. In order to further constrain the properties of the dust in these objects, it is essential to sample the SED as completely as possible. These measurements can then be used to derive critical parameters such as the total infrared luminosity and the range of dust temperatures in the objects of interest. In addition, the MIR to FIR luminosity ratio may indicate the relative importance of warm and

hot dust (which is predominantly heated by the AGN) compared to colder dust, which is preferentially heated by star formation.

The *Herschel* key project (Pilbratt et al. 2010) "The Dusty Young Universe" (PI K. Meisenheimer) aims to measure the FIR SEDs for all quasars with $z > 5$ that were known at the time of submission of the proposal (early 2007) with the PACS (Poglitsch et al. 2010) and SPIRE (Griffin et al. 2010) instruments. Together with existing NIR and MIR photometry, measurements in five *Herschel* bands will yield complete infrared SED coverage of more than two decades in wavelength. Thus, the properties of the dust and the possible interplay between black-hole growth and galaxy bulge formation (traced indirectly through the FIR emission) can be explored early in the evolution of the universe.

2. Observations and data reduction

During the Science Demonstration Phase (SDP) two of our objects with good ancillary data were observed with PACS. No SPIRE point-source photometry of the sources was obtained during the SDP. The objects were selected as SDP targets because they were known to be bright at (sub)mm wavelengths. This allows us to study the performance of *Herschel*/PACS at low flux levels, and the experience gained here will be beneficial in the further course of the project when *Herschel* will be the only source of FIR data for many object. The observations also demonstrate *Herschel*'s ability to detect dust emission at the highest redshifts.

SDSS J1148+5251. The quasar SDSS J1148+5251 at $z = 6.42$ (Fan et al. 2003, hereafter J1148+5251) was observed in

^{*} *Herschel* is an ESA space observatory with science instruments provided by European-led Principal Investigator consortia and with important participation from NASA

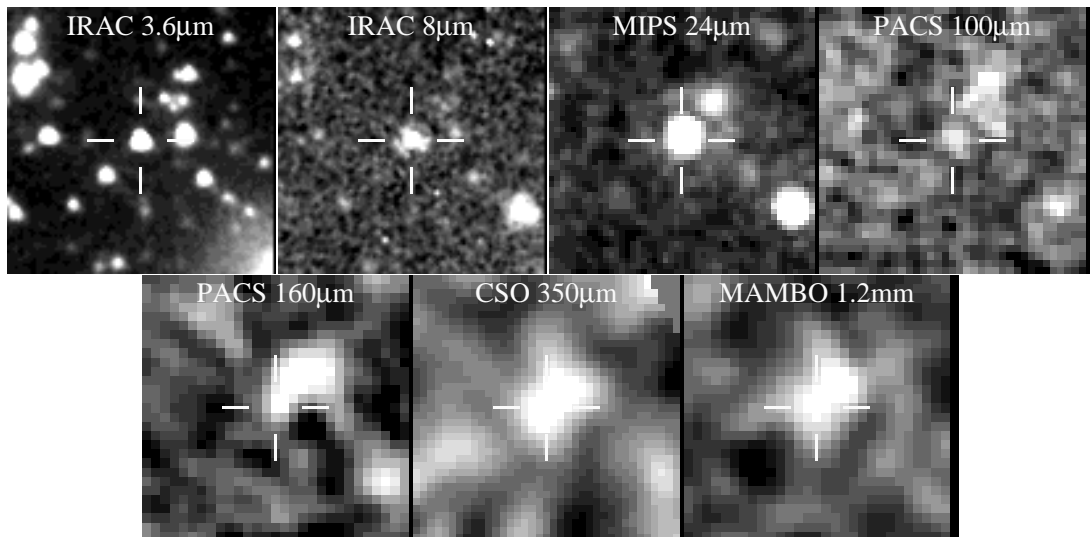


Fig. 1. Infrared and (sub)mm images of J1148+5251. All images are $60''$ wide and north is up with east to the left. Another nearby source northwest of the QSO (see text) is clearly visible at longer wavelengths.

PACS scan-map mode using two cross scans in the green ($100\mu\text{m}$, FWHM $\sim 6''.7$) and in the red ($160\mu\text{m}$, FWHM $\sim 11''$) band (Poglitsch et al. 2010), yielding an effective on-source time of ~ 1150 sec in 3810 sec of total AOR length. We employed standard processing procedures and masked the source location during deglitching and high-pass filtering. Both scan directions were processed separately and were then combined into a single map. The fluxes quoted in this paper were determined using an aperture of $5''.0$ radius (to avoid contaminations from neighbouring sources) and the sky was measured between $30''$ and $35''$. Appropriate aperture corrections were included (Poglitsch et al. 2010)¹. Due to the faintness of the source the fluxes measured via aperture photometry in the final maps were quite sensitive to the parameters chosen during the processing (i.e. the width of the high-pass filter and the size of the masked regions). In addition to the scan maps, the source was also observed in chop-nod mode (~ 2100 sec on-source time). Despite the higher noise levels in the chop-nod observations, the source is securely detected at $100\mu\text{m}$ (but not at $160\mu\text{m}$). The scan maps with high-pass filter widths of 15 and 20 in the green and red bands, respectively, yield fluxes that agree with the chop-nod observations.

BR 1202–0725. The $z = 4.69$ quasar BR 1202–0725 (McMahon et al. 1994, hereafter 1202–0725) was observed in chop-nod mode in the blue ($70\mu\text{m}$, FWHM $\sim 5''.5$) and red band of the PACS instrument for a total of 2550 sec (AOR length) with an on-source time of ~ 1980 sec. Standard processing steps for chop-nod observations were used in combination with the latest calibration information. We performed aperture photometry using apertures with a radius of $7''.0$ and $10''.0$ in the blue and red filters, respectively. The sky was measured at distances between $30''$ and $35''$ away from the source.

3. Results

3.1. J1148+5251

The QSO J1148+5251 at $z = 6.42$ is one of the highest redshift quasars known to date. It has been detected previously at several sub-mm (Beelen et al. 2006; Robson et al. 2004) and

mm (Bertoldi et al. 2003; Riechers et al. 2009) wavelengths. Under the assumption that the heating of the cold dust is dominated by young stars, the high FIR luminosity ($L_{\text{FIR}} \sim 2 \times 10^{13} L_{\odot}$, Beelen et al. 2006) translates into a star-formation rate of $\sim 3000 M_{\odot} \text{yr}^{-1}$. These high star-formation rates are corroborated by measurements of the [C II] emission line at $158\mu\text{m}$ (Maiolino et al. 2005; Walter et al. 2009). Mid-infrared observations (Hines et al. 2006; Jiang et al. 2006) show large amounts of hot dust near the $\sim 3 \times 10^9 M_{\odot}$ black hole which accretes close to its Eddington limit (Willott et al. 2003; Barth et al. 2003).

Figure 1 summarises the available multi-wavelength observations in this field. A careful inspection of the data for J1148+5251 shows a companion $\sim 10''$ to the northwest of the QSO in the FIR (this is best seen in the $160\mu\text{m}$ filter). Indeed, a similar extension is seen in the SHARC II observations (Beelen et al. 2006) and in new MAMBO measurements (based on Bertoldi et al. 2003) of the source. The confusing source is clearly identified in many bands presented here, and a preliminary analysis of deep HST/ACS imaging of this field does not reveal an obvious counterpart. Interferometric maps at ~ 1 mm obtained at IRAM/PdBI (Walter et al. 2009) do not show a counterpart for the companion source. However, the observations were centred on the QSO, which places the location of the companion just outside of the primary beam at that wavelength, thus resulting in highly reduced sensitivity. Given the currently available data on this source it is clear that further studies will be needed to reveal its true nature. We note though that depending on the shape of its SED this additional source will affect measurements

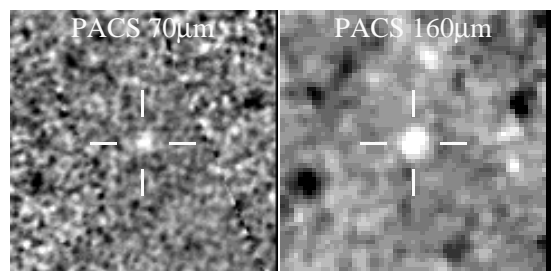


Fig. 2. *Herschel*/PACS chop-nod images of BR 1202–0725. The images are $120''$ wide and north is up with east to the left.

¹ see also the PACS Photometer release note available on the *Herschel* Science Centre website <http://herschel.esac.esa.int/>

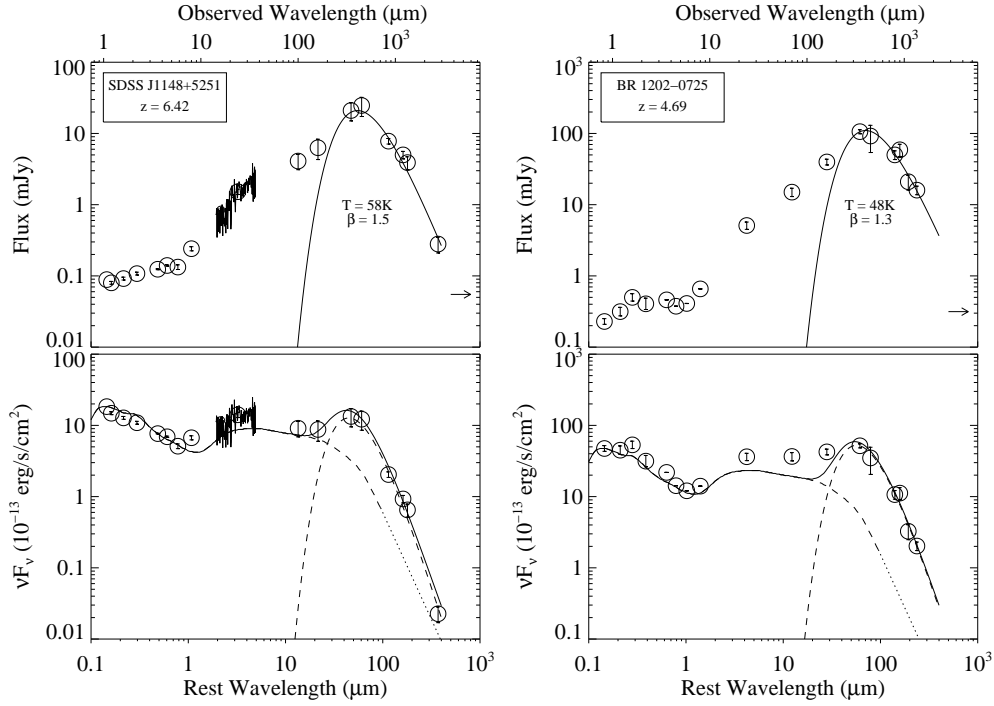


Fig. 3. Spectral flux distributions (*top*) and spectral energy distributions (*bottom*) for J1148+5251 (*left*) and for 1202–0725 (*right*). The arrow indicates the level of the 1.4 GHz (observed frame) radio emission (Tab. 1). In the top plot the solid line shows a single temperature grey body fit to the data at $\lambda_{\text{obs}} > 160 \mu\text{m}$. In the bottom panels we show as dashed lines the same greybody and also the mean SED for optically-luminous SDSS QSOs (Richards et al. 2006), scaled to the 1450 \AA (rest frame) data point. The mean SED was extrapolated for wavelengths longer than $100 \mu\text{m}$ (rest frame) assuming $F_\nu \sim \nu^2$ (dotted line). The solid line is the sum of the scaled SED and the fitted greybody. Both objects clearly show a large excess of cold dust emission ($\lambda \gtrsim 30 \mu\text{m}$, rest frame) compared to the mean QSO template. For J1148+5251 we here also include a *Spitzer*/IRS spectrum, which we retrieved from the archive and processed in a standard manner.

of J1148+5251 done with large ($\gtrsim 10''$) beams. Aperture photometry of J1148+5251 yields a flux density at 100 and $160 \mu\text{m}$ of $4.1 \pm 1.0 \text{ mJy}$ and $6.3 \pm 2.0 \text{ mJy}$, respectively (see Table 1 for a summary of all flux measurements, including literature data). In the red band we removed the confusing source via PSF fitting prior to performing the photometry.

3.2. BR 1202–0725

BR 1202–0725 is a well studied quasar at $z = 4.69$ with strong detections at sub-mm and mm wavelengths (Isaak et al. 1994; Omont et al. 1996b; Benford et al. 1999; Iono et al. 2006) and in CO line emission (Ohta et al. 1996; Omont et al. 1996a; Carilli et al. 2002). At $\sim 4''$ distance to the northwest of the quasar this source shows a secondary component in the dust continuum and in CO. A Ly α extension is observed approximately $2''.3$ northwest of the quasar (Petitjean et al. 1996; Hu et al. 1996; Fontana et al. 1998; Ohya et al. 2004). We detected BR 1202–0725 at $70 \mu\text{m}$ and $160 \mu\text{m}$ with fluxes of $15.0 \pm 2.0 \text{ mJy}$ and $39.8 \pm 3.7 \text{ mJy}$, respectively (Fig. 2), which is consistent with the upper limits from ISO (Leech et al. 2001). In their *Spitzer* observations at $24 \mu\text{m}$, Hines et al. (2006) see slightly resolved emission and perform a two-component PSF fit to isolate the emission attributable to the QSO. Although our PACS $70 \mu\text{m}$ data have slightly higher resolution than the MIPS $24 \mu\text{m}$ observations, we do not detect a secondary component securely, probably due to the lower S/N in the $70 \mu\text{m}$ maps compared to the $24 \mu\text{m}$ image. Although an apparent elongation may be visible for the red band in Fig. 2, a two-component fit does not give

a significantly better fit to the source profile. As we cannot reliably separate the two sources in the PACS observations, the quoted flux values refer to the sum of both components.

4. Discussion and conclusion

In Fig. 3 we show the spectral flux and energy distributions of J1148+5251 and 1202–0725. The SEDs of both high-redshift QSOs appear very similar in shape, and the strong emission in all infrared bands shows dust at a wide range of temperatures. This is particularly emphasised by the *Herschel* photometry, which fills the gap between the previously available MIR and sub-mm photometry. The shape of the SED also implies that large amounts of dust are present in the host galaxies already at high redshift and that the dust may be distributed on a wide range of scales: NIR emission from hot dust close to the nucleus (e.g. Hines et al. 2006; Jiang et al. 2006, 2010), warm MIR dust ($T \sim \text{few hundred K}$) on intermediate scales (or partly shielded), and colder dust in the FIR possibly distributed throughout the host galaxy. Using the new *Herschel* photometry to determine total infrared luminosities for these two objects (integrating the SEDs between 1 and $200 \mu\text{m}$, rest frame) yields $L_{\text{FIR}} = 8.1 \times 10^{13} L_\odot$ for J1148+5251 and a total $L_{\text{FIR}} = 3.7 \times 10^{14} L_\odot$ for 1202–0725.

The inspection of the spectral energy distributions in Fig. 3 shows that in the UV/optical and NIR/MIR (see below), where the emission is dominated by the active nucleus, the SEDs of the high- z sources match the template SEDs from lower redshift AGN (Richards et al. 2006) reasonably well. However, while the

low- z infrared SEDs show only one broad peak at short MIR wavelengths, we observe a second peak with considerable excess emission at FIR wavelengths in our targets. Greybody fits to the data at $\lambda > 160 \mu\text{m}$ yield a temperature of $\sim 50 - 60 \text{ K}$ for the FIR dust emission, which is likely powered by the vigorous star formation (see also Bertoldi et al. 2003; Beelen et al. 2006; Wang et al. 2008). These large contributions to the FIR emission, which can presumably be attributed to ongoing star formation suggesting rapid bulge build-up in the host galaxies at high redshift, are missing in most lower redshift AGN. A combination of the mean QSO SED and the single temperature greybody representing the contributions from star formation is able to match the observed photometry. We note however that both objects presented here were selected as SDP targets because of their known strong FIR/sub(mm) emission. In principle, they could represent a small fraction of strongly star-forming objects, while the majority of the high- z QSOs may lack such a powerful FIR component. An analogue for this situation may be found in the (mostly local) PG quasars (Haas et al. 2003): when compared to the high- z objects, many of the PG sources show a similar mismatch in the FIR as seen for the SDSS QSO template, but a small number of PG quasars reveal a comparable FIR excess as seen for the high-redshift QSOs. Alternatively, stronger FIR emission from bulge build-up via star formation may be more common at high z than at low z , and we plan to explore these questions once data for a greater number of high-redshift objects become available.

Both QSOs show more flux at NIR and MIR wavelengths than we would expect from the local templates. For 1202–0725 this may be understood to be due to the inclusion of the companion (which is at the same redshift as the quasar; Omont et al. 1996a, Carilli et al. 2002) and which contributes roughly half of the flux in many infrared and (sub)mm bands (e.g. Omont et al. 1996a; Hines et al. 2006; Iono et al. 2006). For J1148+5251 the situation is somewhat different, because the QSO is clearly the dominating source in flux at e.g. 8 and $24 \mu\text{m}$ (observed, Fig. 1). However, the exceptionally luminous black hole in this QSO accretes close to its Eddington limit, which could possibly lead to a larger fraction of dust being heated to high temperatures, resulting in increased NIR emission.

For both objects a secondary component may contribute to the measured flux densities at FIR wavelengths, potentially leading to an overestimate of the FIR luminosity of the QSO itself.

Acknowledgements. PACS has been developed by a consortium of institutes led by MPE (Germany) and including UVIE (Austria); KU Leuven, CSL, IMEC (Belgium); CEA, LAM (France); MPIA (Germany); INAF/IFSI/OAA/OAP/OAT, LENS, SISSA (Italy); IAC (Spain). This development has been supported by the funding agencies BMVIT (Austria), ESA-PRODEX (Belgium), CEA/CNES (France), DLR (Germany), ASI/INAF (Italy), and CICYT/MCYT (Spain). M.H. is supported by the Nordrhein-Westfälische Akademie der Wissenschaften und der Künste. D.H. is supported by F.R.S.-FNRS (Belgium). We thank the referee for useful comments that helped to improve the paper.

References

- Barth, A. J., Martini, P., Nelson, C. H., & Ho, L. C. 2003, *ApJ*, 594, L95
 Beelen, A., Cox, P., Benford, D. J., Dowell, C. D., Kovács, A., Bertoldi, F., Omont, A., & Carilli, C. L. 2006, *ApJ*, 642, 694
 Benford, D. J., Cox, P., Omont, A., Phillips, T. G., & McMahon, R. G. 1999, *ApJ*, 518, L65
 Bertoldi, F., Carilli, C. L., Cox, P., Fan, X., Strauss, M. A., Beelen, A., Omont, A., & Zylka, R. 2003, *A&A*, 406, L55
 Carilli, C. L., et al. 2002, *AJ*, 123, 1838
 Carilli, C. L., et al. 2004, *AJ*, 128, 997
 Cohen, M., Wheaton, W. A., & Megeath, S. T. 2003, *AJ*, 126, 1090
 Fan, X., et al. 2003, *AJ*, 125, 1649

Table 1. Multi-wavelength data. All fluxes are given in mJy.

| λ_{obs} in μm | SDSS J1148+5251 $z = 6.42$ | refs | BR 1202–0725 $z = 4.69$ | refs |
|--|-------------------------------|------|----------------------------|------|
| 0.1450 ^a | 0.0887 | 1 | 0.23±0.02 | 11 |
| 1.2 | 0.080±0.004 ^b | 1 | 0.32±0.04 ^b | 12 |
| 1.6 | 0.092±0.004 ^b | 2 | 0.50±0.06 ^b | 12 |
| 2.2 | 0.11±0.005 ^b | 2 | 0.41±0.08 ^b | 12 |
| 3.6 | 0.124±0.002 | 3 | 0.461±0.001 | 4 |
| 4.5 | 0.140±0.003 | 3 | 0.375±0.001 | 4 |
| 5.8 | 0.133±0.010 | 3 | 0.410±0.001 | 4 |
| 8.0 | 0.241±0.016 | 3 | 0.657±0.002 | 4 |
| 16.0 | 0.84 | 3 | – | – |
| 24.0 | 1.520±0.130 | 4 | 5.1±0.6 ^c | 5 |
| 70.0 | – | – | 15.0±2.0 ^c | 5 |
| 100.0 | 4.1±1.0 | 5 | – | – |
| 160.0 | 6.3±2.0 | 5 | 39.8±3.7 ^c | 5 |
| 350.0 | 21±6 | 6 | 106±7 ^c | 13 |
| 450.0 | 24.7±7.4 | 7 | 92±38 ^c | 14 |
| 800.0 | – | – | 50±7 ^c | 14 |
| 850.0 | 7.9±0.7 | 7 | – | – |
| 900.0 | – | – | 59±11 ^c | 15 |
| 1100.0 | – | – | 21±5 ^c | 14 |
| 1200.0 | 5.0±0.6 | 8 | – | – |
| 1330.0 | 3.9±0.8 | 9 | – | – |
| 1350.0 | – | – | 16.0±2.2 ^c | 16 |
| 2750.0 | 0.28±0.07 | 9 | – | – |
| 1.4 GHz | 0.055±0.8 | 10 | 0.315±0.080 ^c | 17 |

(^a) Refers to the 1450 Å flux in the rest frame of the source.

(^b) Calculated using the zero points presented in Cohen et al. (2003).

(^c) Total flux including the companion.

References. (1) Fan et al. 2003; (2) Iwamuro et al. 2004; (3) Jiang et al. 2006; (4) Hines et al. 2006; (5) this work; (6) Beelen et al. 2006; (7) Robson et al. 2004; (8) Bertoldi et al. 2003; (9) Riechers et al. 2009; (10) Carilli et al. 2004; (11) Storrie-Lombardi et al. 1996; (12) Skrutskie et al. 2006; (13) Benford et al. 1999; (14) Isaak et al. 1994; (15) Iono et al. 2006; (16) Omont et al. 1996a; (17) Yun et al. 2000.

- Fontana, A., D’Odorico, S., Giallongo, E., Cristiani, S., Monnet, G., & Petitjean, P. 1998, *AJ*, 115, 1225
 Griffin et al. 2010, this volume
 Haas, M., et al. 2003, *A&A*, 402, 87
 Hines, D. C., Krause, O., Rieke, G. H., Fan, X., Blaylock, M., & Neugebauer, G. 2006, *ApJ*, 641, L85
 Hu, E. M., McMahon, R. G., & Egami, E. 1996, *ApJ*, 459, L53
 Iono, D., et al. 2006, *ApJ*, 645, L97
 Isaak, K. G., McMahon, R. G., Hills, R. E., & Withington, S. 1994, *MNRAS*, 269, L28
 Iwamuro, F., Kimura, M., Eto, S., Maihara, T., Motohara, K., Yoshii, Y., & Doi, M. 2004, *ApJ*, 614, 69
 Jiang, L., et al. 2006, *AJ*, 132, 2127
 Jiang, L., et al. 2010, *Nature*, 464, 380
 Leech, K. J., Metcalfe, L., & Altieri, B. 2001, *MNRAS*, 328, 1125
 Maiolino, R., et al. 2005, *A&A*, 440, L51
 McMahon, R. G., Omont, A., Bergeron, J., Kreysa, E., & Haslam, C. G. T. 1994, *MNRAS*, 267, L9
 Ohta, K., Yamada, T., Nakanishi, K., Kohno, K., Akiyama, M., & Kawabe, R. 1996, *Nature*, 382, 426
 Ohya, Y., Taniguchi, Y., & Shioya, Y. 2004, *AJ*, 128, 2704
 Omont, A., Petitjean, P., Guilloteau, S., McMahon, R. G., Solomon, P. M., & Pécontal, E. 1996a, *Nature*, 382, 428
 Omont, A., McMahon, R. G., Cox, P., Kreysa, E., Bergeron, J., Pajot, F., & Storrie-Lombardi, L. J. 1996b, *A&A*, 315, 1
 Petitjean, P., Pécontal, E., Valls-Gabaud, D., & Chariot, S. 1996, *Nature*, 380, 411
 Pilbratt et al. 2010, this volume
 Poglitsch et al. 2010, this volume
 Richards, G. T., et al. 2006, *ApJS*, 166, 470
 Riechers, D. A., et al. 2009, *ApJ*, 703, 1338

- Robson, I., Priddey, R. S., Isaak, K. G., & McMahon, R. G. 2004, MNRAS, 351, L29
- Skrutskie, M. F., et al. 2006, AJ, 131, 1163
- Storrie-Lombardi, L. J., McMahon, R. G., Irwin, M. J., & Hazard, C. 1996, ApJ, 468, 121
- Walter, F., Riechers, D., Cox, P., Neri, R., Carilli, C., Bertoldi, F., Weiss, A., & Maiolino, R. 2009, Nature, 457, 699
- Wang, R., et al. 2008, ApJ, 687, 848
- Willott, C. J., McLure, R. J., & Jarvis, M. J. 2003, ApJ, 587, L15
- Yun, M. S., Carilli, C. L., Kawabe, R., Tutui, Y., Kohno, K., & Ohta, K. 2000, ApJ, 528, 171